ACS APPLIED MATERIALS & INTERFACES

Research Article

www.acsami.org

Interfacial Alkali Diffusion Control in Chalcopyrite Thin-Film Solar Cells

Shogo Ishizuka,* Akimasa Yamada, Paul J. Fons, Hajime Shibata, and Shigeru Niki

National Institute of Advanced Industrial Science and Technology, 1-1-1 Umezono, Tsukuba, Ibaraki 305-8568, Japan

Supporting Information

ABSTRACT: Alkali elements, specifically sodium (Na), are key materials to enhance the energy conversion efficiencies of chalcopyrite and related thin-film photovoltaic solar cells. Recently, the effect of potassium (K) has also attracted attention because elemental K has unique effects different from Na as well as a similar beneficial effect in improving device performance. In this study, the control of selective alkali K and Na diffusion into chalcopyrite thin-films from soda-lime glass substrates, which serve as the monolithic alkali source material and contain both K and Na, is demonstrated using ternary $CuGaSe_2$. Elemental K is found to be incorporated in the several ten nanometer thick Cu-deficient region, which is formed on the $CuGaSe_2$ film surface, while Na is ejected, although both K and Na diffuse from the substrate to the $CuGaSe_2$ film surface during growth. The alkali [K]/[Na] concentration ratio in the surface region of $CuGaSe_2$ films strongly depends on the film structure and can be controlled by growth parameters under the same substrate temperature conditions. The results we present here offer new concepts necessary to explore and develop emerging new chalcopyrite and related materials and optimize their applications.

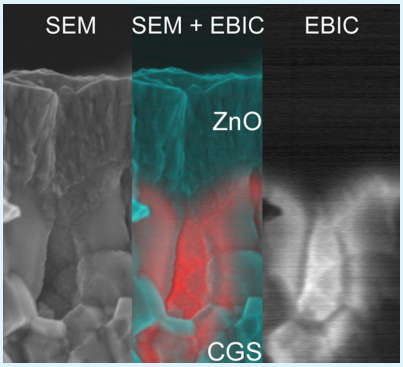

KEYWORDS: *chalcopyrite, photovoltaics, potassium, sodium, thin-films*

1. INTRODUCTION

At the dawn of chalcopyrite $Cu(In,Ga)Se_2$ (CIGS) solar cell devices from the 1970s to the 1990s, single crystals were often used as the photoabsorber layer.[1−4] For example, a $CuGaSe_2$ (CGS) single crystal device was demonstrated with an energy conversion efficiency (η) of 9.7% with an open circuit voltage (V_{oc}) of 0.946 V.[4] These parameters are among the highest values reported to date for ternary CGS solar cells[5−7] despite the absence of alkali elements due to the use of a single crystal of CGS as the photoabsorber. Today, however, alkali elements such as Na are now widely believed to be indispensable dopant impurities in attaining good solar cell performance from CIGS polycrystalline thin-film devices,[8−11] although the detailed mechanism behind the beneficial effects of alkali elements is still open for discussion.[12−14]

Indium-free ternary CGS has the widest band gap energy (E_g) of 1.7 eV among the quaternary CIGS materials and thus is the starting material for wide-gap CIGS devices, which are expected to demonstrate high values of V_{oc} and η. The ideal E_g value is speculated to be about 1.4 eV, corresponding to the [Ga]/([In] + [Ga]) composition ratio of 0.6, for the case of single junction solar cells.[15−17] Recently, relatively wide-gap (1.5−2 eV) materials including CGS have been attracting attention for use in various renewable energy applications such as photoelectrochemical water splitting[18−20] as well as the application as the top cell in multistacked type photovoltaic solar cells.[21,22] The structure of these devices, that is, p−n junctions consisting of p-type and n-type chalcogenide materials, is common regardless of application. As mentioned above, the incorporation of alkali elements is necessary to achieve good device performance from polycrystalline CIGS and related thin-film devices. Effects such as improvements in V_{oc} and fill factor (FF), and concomitant enhancements in the efficiency of solar cell devices, are widely known as the so-called alkali effect. Among the alkali elements, Na has been recognized as being more beneficial than others.[23] In addition to Na, elemental K has recently been given more credit after a report of efficiency enhancements upon potassium fluoride (KF) postdeposition treatments.[11,24] In contrast to the success of the CIGS technology as a practical thin-film photovoltaic industry,[25] there are still many issues that should be resolved regarding fundamental science such as the mechanism behind the p−n junction formation and the physics underlying the role of grain boundaries as well as alkali effects. Such concepts are also necessary to explore and develop emerging new chalcogenide materials and optimize their applications.

In our recent work, ternary CGS polycrystalline thin-film solar cells reached over 10% energy conversion efficiencies by structural tuning of the CGS photoabsorber layers by varying the Se-flux used during film growth.[26] This is the first report of double digit efficiency for elementally In-free chalcopyrite solar cells (see Figure S1, Supporting Information), and the efficiency is higher than that demonstrated from a single crystal CGS device reported in the literature.[3,4] For enhancing

Received: June 2, 2014
Accepted: July 8, 2014
Published: July 8, 2014

the efficiencies of chalcopyrite thin-film solar cells, the control of alkali element incorporation into the photoabsorber layers is definitely a critical issue. In this study, the correlation between the photoabsorber layer structure that can be controlled by varying the Se-flux used during growth and the alkali distribution profiles is investigated. A Cu-deficient region, which appears at CGS surfaces and plays an important role to form a buried p−n junction near the CGS/CdS interface within the CGS layer, is found to incorporate a high concentration of elemental K rather than Na. The distribution control of alkali K and Na in CGS films with a focus on interfaces and the effects on device properties are discussed.

2. EXPERIMENTAL SECTION

Sample Preparation. The CGS and CIGS films were grown on Mo-coated soda-lime glass (SLG) substrates by the three-stage coevaporation process, where Ga_2Se_3 or $(In,Ga)_2Se_3$ precursor films were prepared during the first stage using elemental Se and Ga (and In for In-containing precursors) fluxes at the substrate temperature (T_s) of 350 °C. Elemental Se and Cu fluxes were supplied during the second stage for a T_s of 550 °C, followed by the third stage where elemental Se and Ga (and In for CIGS) were supplied using fluxes identical to those used in the first stage for a T_s of 550 °C. For CGS film growth, the elemental Cu and Ga beam fluxes were kept constant at about 5×10^{-5} Pa, and the Se flux was varied to control the elemental Se to metal Ga or Cu flux ratio $P_{[Se]/[Ga]}$ ($\approx P_{[Se]/[Cu]}$) values during growth. The Se flux was fixed at constant values during all three stages in this study. More details can be found elsewhere.[27] For CIGS film growth, the elemental Cu and ([Ga] + [In]) beam fluxes were kept constant at about 5×10^{-5} and 1×10^{-4} Pa, respectively. The thicknesses of the CGS and CIGS films used in this study were about 1.7 and 2.0 μm, respectively. Solar cell devices were fabricated using chemical bath-deposited CdS buffer layers on CGS films followed by the sputter-deposition of intrinsic and Al-doped ZnO layers.

Solar Cell Parameter Measurements. Solar cell parameters were measured at 25 °C under 100 mW/cm^2 (AM 1.5 G) illumination. An acrylic-film antireflection coating was used for the measurements of selected cells. In-house measurements were performed using an active area of 0.514 cm^2 with an evaporated Al-grid electrode.

Elemental Depth Profile Measurements. The alkali K and Na concentrations in CGS and CIGS films and the corresponding depth profiles of the constituent elements were studied by secondary ion mass spectrometry (SIMS) measurements using Cs^+ as a primary ion with an acceleration voltage of 5 kV. The K and Na concentrations were estimated from secondary ion intensities using a calibration based upon a known standard sample of K and Na ion-implanted CIGS. The estimated values of K and Na concentrations are, therefore, effective only for CIGS in the strict sense, and the concentrations in CGS and Cu-deficient layers are approximate values as shown in the figures containing the SIMS results. We have confirmed, however, that these approximate alkali concentrations estimated in CGS and Cu-deficient layers by SIMS measurements are relatively consistent with values evaluated by energy dispersive X-ray spectroscopy measurements. The unit "cps" used for secondary ion intensity is an abbreviation of "counts per second".

EBIC Measurements. Electron-beam induced current (EBIC) measurements were performed to reveal the position of p−n junctions and the space charge region using various acceleration voltages ranging from 5 to 15 kV.

3. RESULTS

The devices used in this study employed conventional SLG substrates as shown in Figure 1a. Additional postdeposition treatments with alkali fluorides such as NaF or KF were not performed, and thus all of the alkali elements present in photoabsorber layers originate from diffusion from the substrate. The use of CdS as a component of chalcogenide

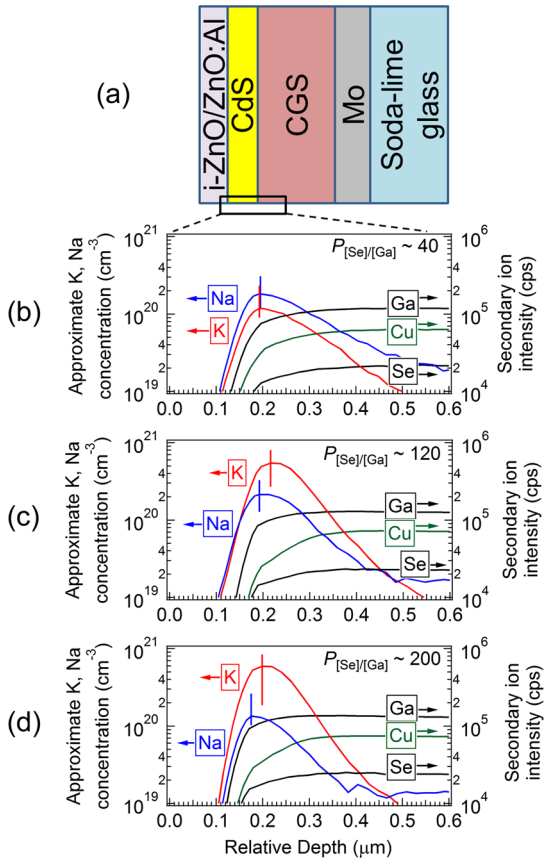

Figure 1. A schematic CGS solar cell device structure (a) and SIMS depth profiles of elemental K, Na, Cu, Ga, and Se near the surface region of CGS layers grown on 1200 nm thick Mo-coated SLG substrates with $P_{[Se]/[Cu]}$ values of 40 (b), 120 (c), and 200 (d). Alkali K and Na concentration peak positions are indicated with vertical lines serving as guides for the eye.

devices such as p-CIGS/n-CdS,[11,24] p-CdTe/n-CdS,[28,29] or p-$Cu_2ZnSn(S,Se)_4$/n-CdS (ref 30) is the most orthodox but promising structure to demonstrate highly efficient solar cells. Although the development of alternative highly efficient Cd-free materials is desired for practical and industrial applications,[25] the current benchmark device structure fabricated with CdS buffer layers is still useful to perform comparative studies on laboratory-scale small area devices, and thus CdS buffer layers are used in this study.

Figure 1b−d shows SIMS depth profiles for elemental K, Na, Cu, Ga, and Se near the CdS/CGS interface in three solar cell devices grown with various Se fluxes. An increase in the elemental K concentration and a decrease in Na concentration with increasing Se-flux used during three-stage coevaporation growth were clearly observed. Here, the elemental Se to metal Ga or Cu flux ratio $P_{[Se]/[Ga]}$ or $P_{[Se]/[Cu]}$ values were controlled by varying the elemental Se beam flux with constant Cu and Ga flux values. As described in the Experimental Section, the $P_{[Se]/[Ga]}$ and $P_{[Se]/[Cu]}$ values used in this study are almost same, and thus the Se flux ratio during all three stages is expressed as $P_{[Se]/[Ga]}$ hereafter. With an increase of K concentration, the formation of a Cu-deficient region at the CGS surface is clearly enhanced and the peak position of the elemental K signal shifts to the Cu-deficient region, although the peak position of the elemental Na signal remains at the CGS surface. Postdeposition surface treatments with potassium compounds are known to

lead to the formation of a Cu-deficient region on the film surface.[11] On the other hand, the result shown in Figure 1c,d suggests that elemental K, which diffuses from the substrate, also contributes to form Cu-deficient regions on the film surface.

The trade-off variation observed in the elemental [K]/[Na] concentration ratio in CGS films, that is, an increase in elemental K and a decrease in Na concentration with increasing $P_{[Se]/[Ga]}$ values during growth, is also observed for various thicknesses of Mo back contact layers. Figure 2a,b shows the

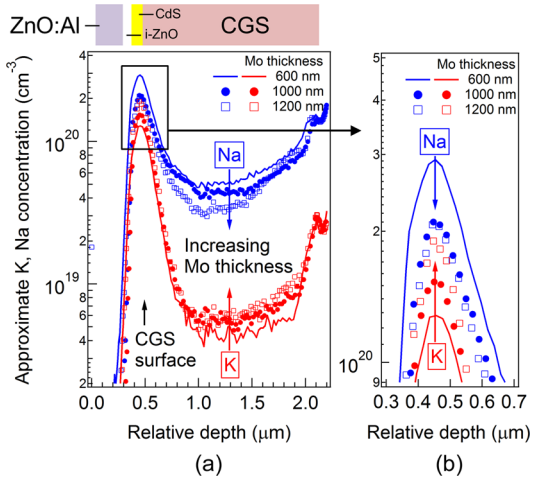

Figure 2. SIMS depth profiles of elemental K and Na in CGS layers grown on SLG substrates with various Mo thicknesses (a). The CGS films were grown in an identical deposition run with the use of the $P_{[Se]/[Ga]}$ value of 30. The elemental K and Na profiles near the CGS surface are magnified in the rectangular-marked region (b).

variation in the elemental K and Na concentrations in CGS films with Mo thicknesses ranging from 600 to 1200 nm. The use of thicker Mo layers leads to a decrease of Na diffusion, whereas the K concentration in CGS films increases. The CGS film structure changes with the $P_{[Se]/[Ga]}$ values used during growth, and the use of high $P_{[Se]/[Ga]}$ values enhances the formation of small grain regions and hence the porosity in the lower part of films as shown in Figure 3a,b (surface SEM images for these CGS films are shown in Figure S2, Supporting Information). The concentration of alkali elements tends to increase in the small grain region as shown in Figure 3c, implying that alkali elements are present at the grain boundaries rather than in the bulk crystal. Figure 3d shows elemental O distribution profiles in CGS films observed from the same CGS devices shown in Figures 2a and 3c. It has been reported in the literature that there is no significant correlation between the presence of elemental Na and O in CIGS films when Na is doped using NaF as a precursor,[31] although the use of NaF precursors has been suggested to promote the formation of MoO_3 and $MoSe_2$ compounds on the Mo back contact surface.[32] The elemental O distribution profiles in the CGS layers shown in Figure 3d, however, clearly correlate with the profiles of Na and are independent of the K distribution profiles. The variation in the elemental K, Na, and O concentrations observed with increasing Mo thickness shown in Figures 2a and 3d is consistent with the result observed with increasing $P_{[Se]/[Ga]}$ value. These results indicate that elemental Na, which diffuses from the SLG substrate into the CGS film, is accompanied by oxygen. This is different from the case for Na doping with the use of NaF. Although the observation of beneficial effects similar to those due to alkali element incorporation in chalcopyrite thin-films can be expected regardless of the type of alkali source materials used, these results suggest that the alkali diffusion pathway and concomitant secondary effects caused by oxygen depend on the alkali doping method used and may affect film and device properties. From these results, group VI elements are suggested to play the important role of alkali diffusion control. The formation of Na_2Se and K_2Se compounds and their effects on CGS grain growth should be further investigated to clarify the relationship between $P_{[Se]/[Ga]}$ values and selective diffusion of alkali species. On the other hand, the reason for an increase in the K concentration with the use of thicker Mo layers is attributable to the high reactivity of Mo with oxygen. Elemental O diffusing from substrates may be trapped in the Mo layer with Na, and thus the use of thicker Mo layers interferes with Na diffusion into CGS layers while K diffusion into CGS layers is enhanced with thicker Mo layers.

Table 1 summarizes typical solar cell parameters obtained from the devices shown in Figures 2 and 3 with an

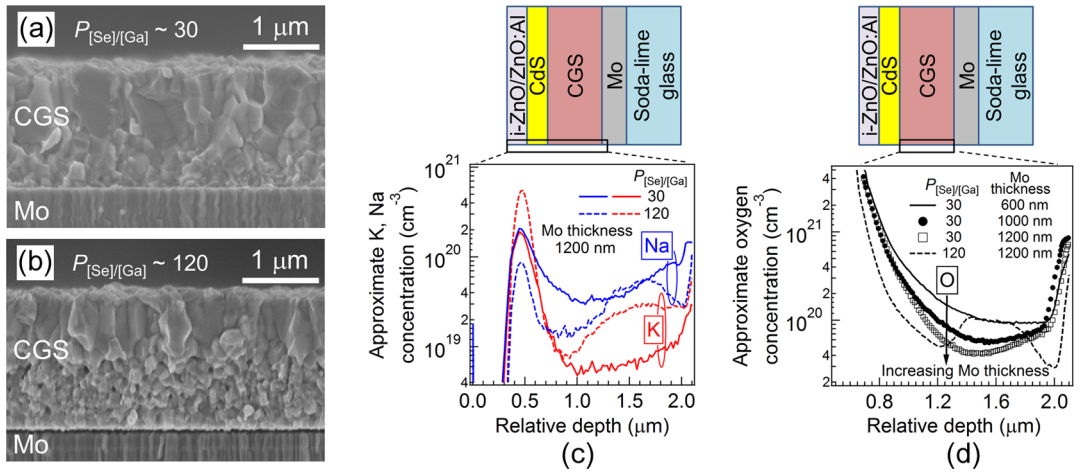

Figure 3. Cross-sectional scanning electron microscopy (SEM) images for CGS films grown on 1200 nm thick Mo-coated SLG substrates with the $P_{[Se]/[Ga]}$ values of 30 (a) and 120 (b). SIMS depth profiles of elemental K and Na obtained from solar cell devices fabricated with these CGS films (c). Elemental O profiles obtained from CGS devices shown in Figures 2a and 3c (d).

dx.doi.org/10.1021/am503480m | ACS Appl. Mater. Interfaces 2014, 6, 14123−14130

Table 1. Solar Cell Parameters Obtained by In-House Measurements from the CGS Devices Shown in Figures 2 and 3 with an Anti-Reflection Coating

Mo thickness (nm)	$P_{[Se]/[Ga]}$	η (%)	V_{oc} (V)	J_{sc} (mA/cm^2)	FF
600	30	8.11	0.858	14.52	0.651
1000	30	9.71	0.890	15.78	0.696
1200	30	10.31	0.914	16.20	0.691
1200	120	10.19	0.875	17.02	0.684

antireflection (AR) coating (diode parameters obtained from these devices are listed in Table S1, and current density–voltage curves measured without an AR coating and external quantum efficiency curves can be found in Figure S3, Supporting Information). The trend of increasing V_{oc} with increasing elemental K concentration observed in Table 1 is consistent with the effects of elemental K on CIGS devices reported in the literature,[24] although the excessively high K concentration induced with the use of the high $P_{[Se]/[Ga]}$ value of 120 led to degradation in V_{oc} and FF. The formation of Cu-deficient phases on the CGS film surface is expected to increase E_g at the film surface and contributes to increase the value of V_{oc}, although it may depend on the carrier concentration and thickness of the Cu-deficient layers. Unlike the case for postdeposition treatments with alkali fluorides, all alkali elements originate and diffuse from the SLG substrate in this study and thus affect the CGS film structure during growth. The increase in J_{sc} observed with increasing elemental K concentration was found to be correlated with CGS film porosity and hence affect the magnitude of CdS diffusion into the CGS. This issue will be discussed later.

In contrast to ternary CGS, the Cu-deficient layer formed on quaternary CIGS film surfaces tends to be remarkably thin as shown in Figure 4. It is generally known that the diffusion coefficient of elemental In in CIGS is higher than Ga (ref 33), and thus the presence of elemental In may suppress the formation of the Cu-deficient layer due to the enhanced migration of elemental Cu with In during the third stage of film growth. In other words, the use of ternary CGS clarified the relationship between the alkali elements and the formation of a Cu-deficient region in this study.

The selective diffusion of alkali K and Na elements from SLG/Mo substrates to CGS films was found to occur during the very initial stage of film growth. In the three-stage coevaporation process of CGS films, a binary Ga_2Se_3 film is prepared during the first stage. The morphology and texture of the Ga_2Se_3 films depend on the $P_{[Se]/[Ga]}$ values[27] as shown in Figure 5a–d. It was found that dense Ga_2Se_3 films prepared with the relatively low $P_{[Se]/[Ga]}$ values around 30 enhanced the diffusion of elemental Na and suppressed the diffusion of K as shown in Figure 5e. On the other hand, porous Ga_2Se_3 films prepared with high $P_{[Se]/[Ga]}$ values of over 100 were found to enhance the diffusion of K and suppress the diffusion of Na as shown in Figure 5f. This trend is consistent with the variation of the [K]/[Na] concentration ratio in CGS films observed with various $P_{[Se]/[Ga]}$ values and implies that the Ga_2Se_3 precursor critically affects the alkali concentration in completed CGS films.

As mentioned above, the $P_{[Se]/[Ga]}$ values used during growth affect CGS film morphology, grain size, and porosity, and concomitant alkali distribution profiles in the films, although no significant variation is observed in the surface appearance.[27] As a consequence, the distribution of Cd and S in CGS films is found to be strongly influenced by the $P_{[Se]/[Ga]}$ values used. Here, a CdS layer is chemical-bath deposited on the CGS film surface for device fabrication as described in the Experimental Section. Figure 6a,b shows elemental Cd and S depth profiles in CGS films grown with the $P_{[Se]/[Ga]}$ values of 30 and 120, respectively. These SIMS profiles were measured using devices nominally identical to those used in Figure 3c. Significant CdS diffusion in CGS films can be observed with the use of $P_{[Se]/[Ga]}$ values of over 100 due to enhanced film porosity with an increase of elemental K as shown in Figure 6b. A similar trend can be observed in the CGS films shown in Figure 2, where the

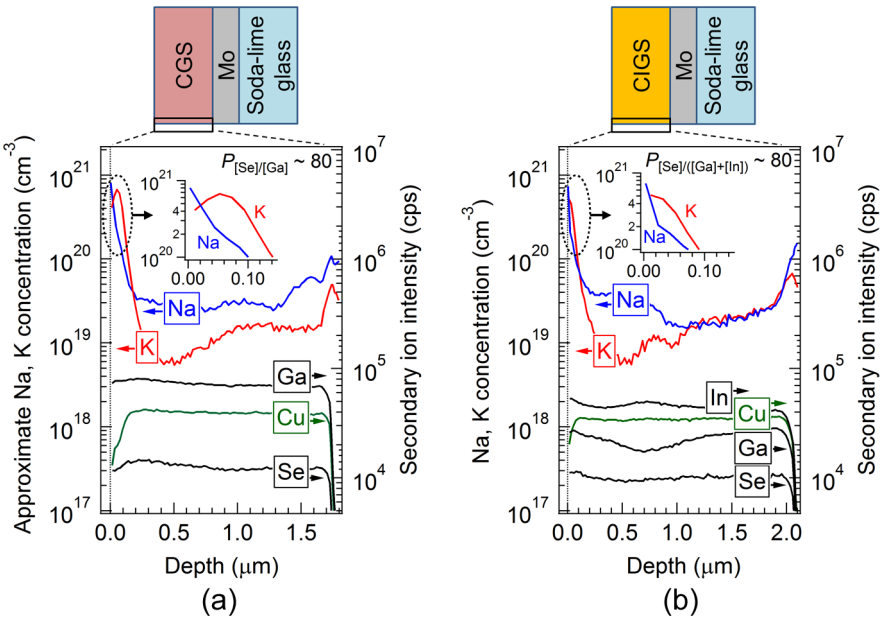

Figure 4. SIMS depth profiles of elemental K, Na, Cu, In, Ga, and Se in as-grown CGS (a) and CIGS (b) films grown on 1200 nm thick Mo-coated SLG substrates with the $P_{[Se]/[Ga]}$ or $P_{[Se]/([In]+[Ga])}$ value of 80. Magnified alkali elemental profiles near the surface region are shown in the inset. The compositional [Ga]/([In] + [Ga]) ratio in the CIGS film is 0.3.

dx.doi.org/10.1021/am503480m | ACS Appl. Mater. Interfaces 2014, 6, 14123–14130

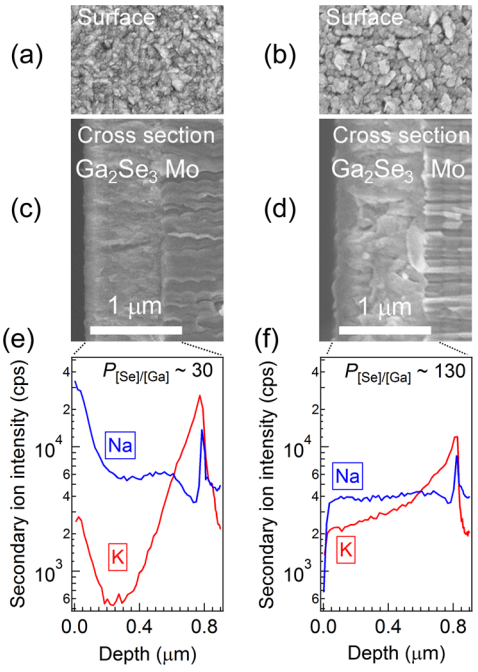

Figure 5. Surface and cross-sectional SEM images for Ga_2Se_3 films grown on 1200 nm thick Mo-coated SLG substrates with the $P_{[Se]/[Ga]}$ values of 30 (a,c) and 130 (b,d). The magnification of the SEM images is identical. SIMS depth profiles of elemental K and Na in these films (e,f).

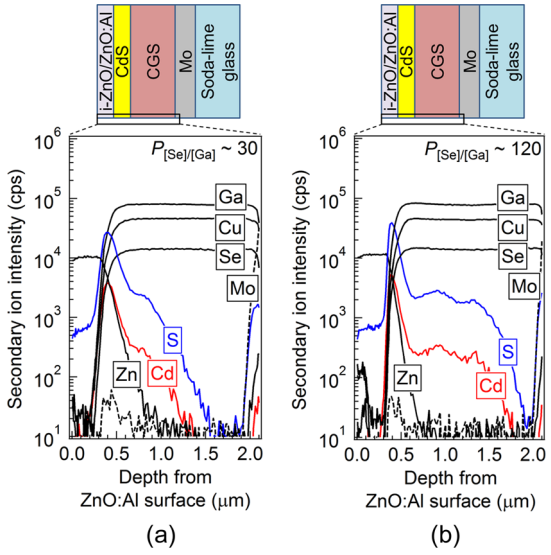

Figure 6. SIMS depth profiles of elemental Cd and S in CGS layers grown with the $P_{[Se]/[Ga]}$ values of 30 (a) and 120 (b).

alkali concentration ratios in the films were controlled by varying the Mo layer thickness (see Figure S4, Supporting Information). Figure 7a–c shows typical EBIC line-scan profiles measured vertically to the constituent layers and typical elemental Cd and S depth profiles for CGS devices grown under a high $P_{[Se]/[Ga]}$ value of over 100 (see also the horizontally measured EBIC profiles shown in Figure S5, Supporting Information). The SIMS depth profile shown in Figure 7c was measured from the substrate side through the CGS layer to the ZnO:Al side to avoid possible signal tails of elemental Cd and S in the CGS layer with the measurements from the surface side. This precaution was, however, over

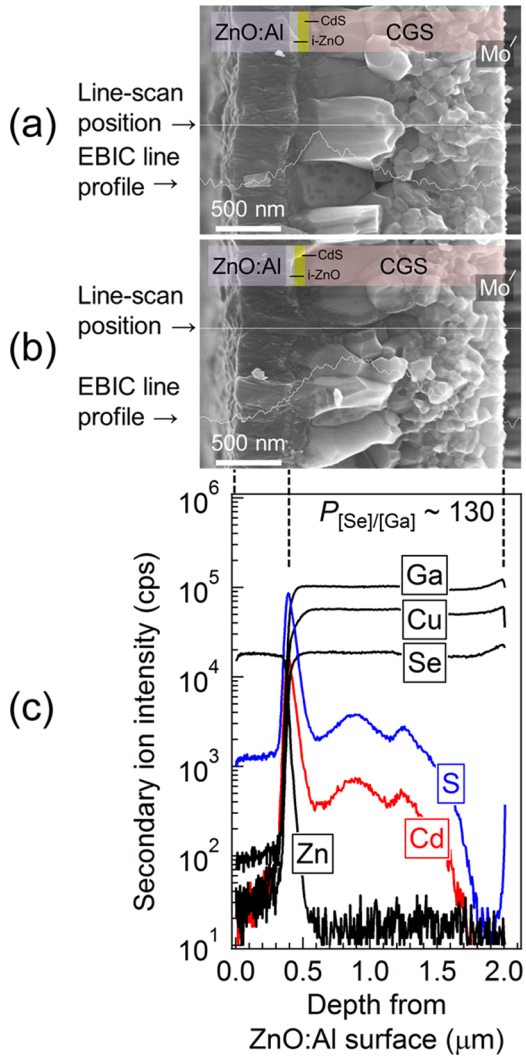

Figure 7. EBIC line-scan profiles measured with an acceleration voltage of 15 kV in the CGS grain (a) and grain boundary (b) in an identical CGS layer grown with a relatively high $P_{[Se]/[Ga]}$ value of 130. Elemental SIMS depth profiles obtained from a corresponding CGS device measured from the substrate side through the CGS layer to the ZnO:Al side (c).

cautious, and the measured SIMS profile was quite similar to that measured from the surface side as shown in Figure 6b. As such, CGS films grown with the use of high $P_{[Se]/[Ga]}$ values or thick Mo back contact layers tend to contain a high K concentration due to the presence of a greater number of diffusion pathway through which Cd and S can diffuse to the CGS film to form a CdS layer. Transmission electron microscopy and energy dispersive X-ray spectroscopy (TEM-EDX) measurements shown in Figure 8a–f represent the elemental distribution profiles in the CGS device shown in Figure 7. The CdS region contained within the CGS film is expected to form a p–n junction at the side of CGS grains as indicated in Figure 7b (see also Figure S5, Supporting Information). In this case, the hole–electron pair generation that leads to the photocurrent generation at the grain boundary is expected to increase. Schematics of the device structure fabricated using CGS films grown with relatively low and high $P_{[Se]/[Ga]}$ values shown in Figure 3a,b are displayed in Figure 9a,b. Although no back surface field effect is expected to repel the minority carriers in ternary CGS photoabsorbers due to the

dx.doi.org/10.1021/am503480m | ACS Appl. Mater. Interfaces 2014, 6, 14123–14130

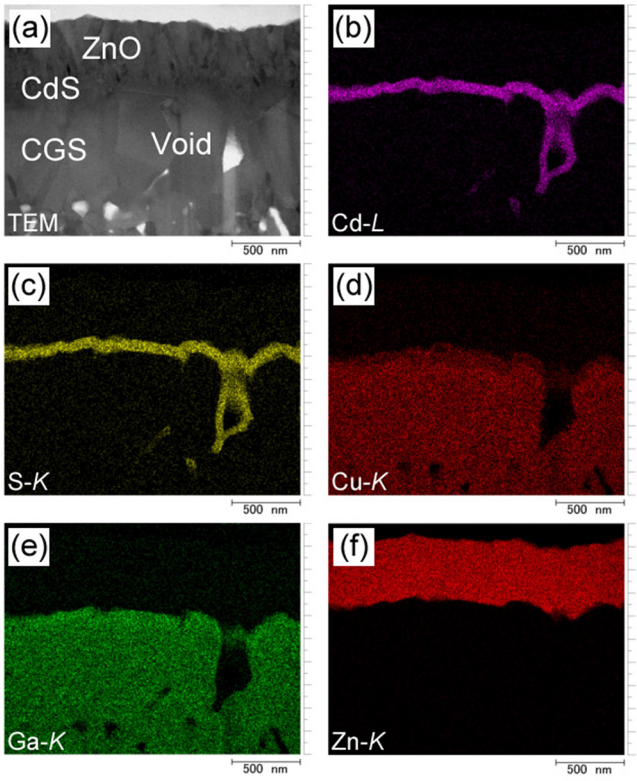

Figure 8. TEM (a) and EDX mappings of elemental Cd (b), S (c), Cu (d), Ga (e), and Zn (f) for a CGS device grown with a $P_{[Se]/[Ga]}$ value of 130. The specimen used is nominally identical to the device shown in Figure 7a–c.

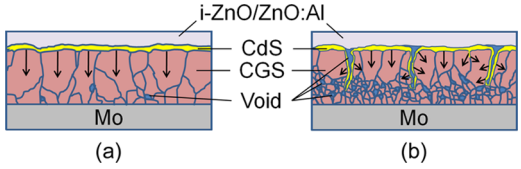

Figure 9. Schematics of cross-sectional CGS solar cell device structures fabricated using CGS films grown with a relatively low $P_{[Se]/[Ga]}$ value about 30 (a) and a relatively high $P_{[Se]/[Ga]}$ value over 100 (b). Arrows indicate the expansion direction of the space charge region in CGS layers.

lack of a [Ga]/[In] compositional gradient, which is generally present in three-stage processed CIGS devices, supplementary carrier generation and collection are expected for the CGS device shown in Figure 9b due to the p–n junction distribution around CGS grain boundaries in the CGS photoabsorber layer. A trend of increasing J_{sc} value with increasing CdS diffusion in CGS films can be observed in Table 1 and Figure 6 (see also Figure S4g, Supporting Information). In our previous work, the Cu-deficient layer present between the CdS and CGS interface was suggested to play the role of an n-type material.[34] The Cu-deficient layer is also suggested to incorporate a high K concentration as shown in Figure 1c,d. These results suggest that elemental K is a beneficial impurity and plays an important role to transport photogenerated carriers in the Cu-deficient layer as well as a role in the formation of Cu-deficient phases on the film surface.

4. DISCUSSION

The formation of Cu-deficient layers on CGS film surfaces with the presence of a large amount of elemental K observed in this study is consistent with the result reported for CIGS films with postdeposition KF surface treatments.[11] In general, alkali elements have been suggested to be incorporated in the Cu-site in CIGS.[11,35,36] In this study, a selective incorporation of elemental K rather than Na into the Cu-deficient layer was clearly observed. It is unreasonable, however, to consider that elemental K, which has about a 2 times larger atomic radius (0.277 nm) than Cu (0.157 nm), easily occupies the Cu-site, although elemental Na has also a large atomic radius of 0.223 nm. Among CIGS compound phases, the Cu-deficient $I–III_3–VI_5$ phase such as $Cu(In,Ga)_3Se_5$ and $CuGa_3Se_5$ is a quite indistinct material as compared to the $I–III–VI_2$ phase because the crystal is not constructed of a rigid unit cell.[37,38] This fact also makes it difficult to perform simulation studies. Our previous work suggests that Cu-deficient phases present on the CGS film surface have an elemental composition close to that of the $I–III_3–VI_5$ phase and play the role of an n-type material.[34] If the structure of the stannite-like $I–III_3–VI_5$ phase is largely different from that of the chalcopyrite $I–III–VI_2$ phase, the formation of Cu-related complex lattice sites where elemental K can be incorporated with a lower formation energy than that for Na might be possible, although further investigation is necessary to discuss and clarify this speculation.

The larger E_g values for the Cu-deficient phases than those of the $I–III–VI_2$ phase are expected to modify the band alignment at the CGS/Cu-deficient CGS/CdS interface.[39] In addition to this, if elemental K plays the role of passivation at CGS grain boundaries as well as Na and increases the hole carrier concentration in the p-type CGS layer, these effects may contribute to increase the V_{oc} values of devices as shown in Table 1. We have observed the presence of a Cu-deficient layer on the surface of CGS films grown with relatively low $P_{[Se]/[Ga]}$ values around 30 as well, although the thickness of the layers is thinner than that for CGS films grown with higher $P_{[Se]/[Ga]}$ values.[27] On the other hand, the deterioration in V_{oc} and FF values observed in Table 1 with the use of a high $P_{[Se]/[Ga]}$ value of over 100 may be due to excessive diffusion of elemental K and a concomitant dramatic variation in film structure such as the presence of crevices, which lead to the formation of nonuniform thickness and thin CGS layer regions.

Space charge regions observed in chalcopyrite thin-film devices occasionally depend on measurement techniques and conditions, and the results are often inconsistent with each other. In our previous work, the depletion layer width observed in CGS layers by capacitance–voltage ($C–V$) measurements with a frequency of 10 kHz showed a clear variation with the $P_{[Se]/[Ga]}$ value used for the CGS growth, and the width decreased from 800 to 300 nm with increasing $P_{[Se]/[Ga]}$ value from 30 to 130 (ref 26). On the other hand, the depletion layer width observed by EBIC measurements was about 1 μm regardless of the $P_{[Se]/[Ga]}$ value.[26] The variation in the depletion layer width observed by $C–V$ measurements is chiefly attributable to two reasons. One possible reason suggested is an increase in the capacitance value due to the formation of thin CGS layer (short CdS–Mo distance) regions when high $P_{[Se]/[Ga]}$ values of over 100 were used. We have observed an increase in capacitance values with increasing $P_{[Se]/[Ga]}$ values. Here, the capacitance C can be expressed as

$$C = \varepsilon_{CGS}\varepsilon_0 S/W \quad (1)$$

where ε_{CGS}, ε_0, S, and W are the dielectric constants of CGS and vacuum, device area, and depletion layer width, respectively. Thin CGS layer regions formed with the presence of crevices on the CGS surface may limit the expansion of the space charge region due to the presence of the small grain region in the lower part of films and result in partly decreased W values (see Figures 3b and 9b, and also Figure S6, Supporting Information). Another possible reason is an increase in the effective device area S of the p−n junction interface distributed at the side of CGS grains in the CGS film grown with high $P_{[Se]/[Ga]}$ values of over 100 as indicated in Figures 7 and 8. As shown in Figure 8f, sputter-deposited ZnO layers are out of contact with the chemical-bath deposited CdS layer distributed in the crevices of the CGS film surface. However, the effective area S, that is, the area of the p−n junction interface, may increase with increasing $P_{[Se]/[Ga]}$ value as shown in Figure 9b. An increase in the effective area S is also expected to contribute to an increase in C values according to eq 1. In C−V measurements, W values were calculated on the premise that the cell device area S is constant. As a consequence, a failure to correctly estimate W values likely occurs and may lead to artificially reduced W values for the CGS device shown in Figure 9b. On the other hand, a similar EBIC image observed for the CGS device shown in Figure 9a to the device shown in Figure 9b is attributed to their nearly identical W values, which represent EBIC images in the large CGS grain region within about 1 μm from the surface of the CGS layers. This can serve as an explanation for the different results seen in the depletion layer width observed by C−V and EBIC measurements. The CGS grain size near the film surface tends to be small for high $P_{[Se]/[Ga]}$ values over 100 in comparison to the grain size in CGS films grown with relatively low $P_{[Se]/[Ga]}$ values ranging from 20 to 40 (ref 27). In our previous work, however, an increase in the J_{sc} value with the use of high $P_{[Se]/[Ga]}$ values was observed despite the relatively small CGS grain sizes in the films.[27] A similar trend can be found in Figure 3a,b and Table 1 in the present work. This result can also explain the enhanced carrier generation in the CGS layer shown in Figure 9b.

5. CONCLUSIONS

In this study, it is found that elemental K, even if it diffuses from the substrate, affects the formation of a Cu-deficient layer on the CGS film surface as well as the film morphology and concomitant device properties. The Cu-deficient layer formed on the CGS film surface has been suggested to have an important role in device performance, and thus the control of the properties of the Cu-deficient layers such as thickness and carrier concentration with alkali element incorporation is expected to open a new frontier for the development of chalcopyrite thin-film device technology. Elemental K, rather than Na, is selectively incorporated into the Cu-deficient layer. It is found that elemental Na diffuses from the substrate into the CGS film along with oxygen, whereas elemental K is independent of oxygen incorporation. The concentration of elemental K and Na is a trade-off relationship, and the K concentration increases with increasing $P_{[Se]/[Ga]}$ value, while the Na concentration decreases, and vice versa. Alkali diffusion in CGS films affects the film structure, which in turn also affects the p−n junction formation in the CGS photoabsorber layers. In this work, elemental K and Na diffusion from the substrate into the CGS film was controlled with independent parameters, that is, $P_{[Se]/[Ga]}$ value and Mo thickness. This result indicates that there are some independent key parameters to control selective alkali K and Na diffusion from the monolithic alkali source material SLG, which contains both K and Na, under the same substrate temperature conditions. The postdeposition KF and NaF treatments currently used for laboratory-scale CIGS solar cells are a promising technique to control the alkali concentration in CIGS films. Nevertheless, the alkali diffusion control technique using conventional SLG substrates can be another promising option for the practical industrial application of CIGS technology.

■ ASSOCIATED CONTENT

Supporting Information

Independently certified photovoltaic performance for the ternary CGS solar cell, SEM images, in-house measured current density−voltage and external quantum efficiency curves, SIMS depth profiles, EBIC profiles, schematic carrier generation and transport model. This material is available free of charge via the Internet at http://pubs.acs.org.

■ AUTHOR INFORMATION

Corresponding Author

*E-mail: shogo-ishizuka@aist.go.jp.

Notes

The authors declare no competing financial interest.

■ ACKNOWLEDGMENTS

We thank M. Iioka, H. Higuchi, S. Kimura, and A. Obara for their help with the experiments and technical support. Financial support by the New Energy and Industrial Technology Development Organization (NEDO) under the Ministry of Economy, Trade and Industry (METI) is greatly acknowledged.

■ REFERENCES

(1) Wagner, S.; Shay, J. L.; Migliorato, P.; Kasper, H. M. $CuInSe_2$/CdS Heterojunction Photovoltaic Detectors. *Appl. Phys. Lett.* **1974**, *25*, 434−435.

(2) Shay, J. L.; Wagner, S.; Kasper, H. M. Efficient $CuInSe_2$/CdS Solar Cells. *Appl. Phys. Lett.* **1975**, *27*, 89−90.

(3) Stankiewicz, J.; Giriat, W. Photovoltaic Effect in Cu/$CuGaSe_2$ Schottky Barriers. *Appl. Phys. Lett.* **1979**, *35*, 70−71.

(4) Saad, M.; Riazi, H.; Bucher, E.; Lux-Steiner, M. Ch. $CuGaSe_2$ Solar Cells with 9.7% Power Conversion Efficiency. *Appl. Phys. A: Mater. Sci. Process.* **1996**, *62*, 181−185.

(5) Young, D. L.; Keane, J.; Duda, A.; AbuShama, J. A. M.; Perkins, C. L.; Romero, M.; Noufi, R. Improved Performance in ZnO/CdS/$CuGaSe_2$ Thin-Film Solar Cells. *Prog. Photovoltaics* **2003**, *11*, 535−541.

(6) Caballero, R.; Kaufmann, C. A.; Cwil, M.; Kelch, C.; Schweigert, D.; Unold, T.; Rusu, M.; Schock, H.-W.; Siebentritt, S. The Role of the CdS Buffer Layer in $CuGaSe_2$-Based Solar Cells. *J. Phys.: Condens. Matter* **2007**, *19*, 356222−1−11.

(7) Contreras, M. A.; Mansfield, L. M.; Egaas, B.; Li, J.; Romero, M.; Noufi, R.; Rudiger-Voigt, E.; Mannstadt, W. Wide Bandgap Cu(In,Ga)Se_2 Solar Cells with Improved Energy Conversion Efficiency. *Prog. Photovoltaics* **2012**, *20*, 843−850.

(8) Hedström, J.; Ohlsén, H.; Bodegård, M.; Kylner, A.; Stolt, L.; Hariskos, D.; Ruckh, M.; Schock, H.-W. ZnO/CdS/Cu(In,Ga)Se_2 Thin Film Solar Cells with Improved Performance. *Conference Record of the 23rd IEEE Photovoltaic Specialists Conference*, Louisville, KY, 1993; pp 364−371.

(9) Ruckh, M.; Schmid, D.; Kaiser, M.; Schäffler, R.; Walter, T.; Schock, H. W. Influence of Substrates on the Electrical Properties of Cu(In,Ga)Se_2 Thin Films. *Conference Record of the 1994 IEEE First*

World Conference on Photovoltaic Energy Conversion, Waikoloa, HI, 1994; pp 156−159.
(10) Rudmann, D.; Cunha, A. F. Da.; Kaelin, M.; Kurdesau, F.; Zogg, H.; Tiwari, A. N.; Bilger, G. Efficiency Enhancement of Cu(In,Ga)Se_2 Solar Cells Due to Post-Deposition Na Incorporation. *Appl. Phys. Lett.* **2004**, *84*, 1129−1131.
(11) Chirilă, A.; Reinhard, P.; Pianezzi, F.; Bloesch, P.; Uhl, A. R.; Fella, C.; Kranz, L.; Keller, D.; Gretener, C.; Hagendorfer, H.; Jaeger, D.; Erni, R.; Nishiwaki, S.; Buecheler, S.; Tiwari, A. N. Potassium-Induced Surface Modification of Cu(In,Ga)Se_2 Thin Films for High-Efficiency Solar Cells. *Nat. Mater.* **2013**, *12*, 1107−1111.
(12) Niles, D. W.; Ramanathan, K.; Hasoon, F.; Noufi, R.; Tielsch, B. J.; Fulghum, J. E. Na Impurity Chemistry in Photovoltaic CIGS Thin Films: Investigation with X-Ray Photoelectron Spectroscopy. *J. Vac. Sci. Technol., A* **1997**, *15*, 3044−3049.
(13) Kronik, L.; Cahen, D.; Schock, H. W. Effects of Sodium on Polycrystalline Cu(In,Ga)Se_2 and Solar Cell Performance. *Adv. Mater.* **1998**, *10*, 31−36.
(14) Ishizuka, S.; Yamada, A.; Islam, M. M.; Shibata, H.; Fons, P.; Sakurai, T.; Akimoto, K.; Niki, S. Na-Induced Variations in the Structural, Optical, and Electrical Properties of Cu(In,Ga)Se_2 Thin Films. *J. Appl. Phys.* **2009**, *106*, 034908-1−6.
(15) Shockley, W.; Queisser, H. J. Detailed Balance Limit of Efficiency of *p-n* Junction Solar Cells. *J. Appl. Phys.* **1961**, *32*, 510−519.
(16) Siebentritt, S. What Limits the Efficiency of Chalcopyrite Solar Cells? *Sol. Energy Mater. Sol. Cells* **2011**, *95*, 1471−1476.
(17) Yu, L.; Zunger, A. Identification of Potential Photovoltaic Absorbers Based on First-Principles Spectroscopic Screening of Materials. *Phys. Rev. Lett.* **2012**, *108*, 068701-1−5.
(18) Moriya, M.; Minegishi, T.; Kumagai, H.; Katayama, M.; Kubota, J.; Domen, K. Stable Hydrogen Evolution from CdS-Modified $CuGaSe_2$ Photoelectrode under Visible-Light Irradiation. *J. Am. Chem. Soc.* **2013**, *135*, 3733−3735.
(19) Marsen, B.; Cole, B.; Miller, E. L. Photoelectrolysis of Water Using Thin Copper Gallium Diselenide Electrodes. *Sol. Energy Mater. Sol. Cells* **2008**, *92*, 1054−1058.
(20) Paracchino, A.; Laporte, V.; Sivula, K.; Grätzel, M.; Thimsen, E. Highly Active Oxide Photocathode for Photoelectrochemical Water Reduction. *Nat. Mater.* **2011**, *10*, 456−461.
(21) Nishiwaki, S.; Siebentritt, S.; Walk, P.; Lux-Steiner, M.; Ch, A. Stacked Chalcopyrite Thin-Film Tandem Solar Cell with 1.2 V Open-Circuit Voltage. *Prog. Photovoltaics* **2003**, *11*, 243−248.
(22) Seyrling, S.; Calnan, S.; Bücheler, S.; Hüpkes, J.; Wenger, S.; Brémaud, D.; Zogg, H.; Tiwari, A. N. $CuIn_{1-x}Ga_xSe_2$ Photovoltaic Devices for Tandem Solar Cell Applicaiton. *Thin Solid Films* **2009**, *517*, 2411−2414.
(23) Contreras, M. A.; Egaas, B.; Dippo, P.; Webb, J.; Granata, J.; Ramanathan, K.; Asher, S.; Swartzlander, A.; Noufi, R. On the Role of Na and Modifications to Cu(In,Ga)Se_2 Absorber Materials using Thin-MF (M=Na, K, Cs) Precursor Layers. *Conference Record of the 26th IEEE Photovoltaic Specialists Conference*, Anaheim, CA, 1997; pp 359−362.
(24) Jackson, P.; Hariskos, D.; Wuerz, R.; Wischmann, W.; Powalla, M. Compositional Investigation of Potassium Doped Cu(In,Ga)Se_2 Solar Cells with Efficiencies up to 20.8%. *Phys. Status Solidi RRL* **2014**, *3*, 219−222.
(25) Solar Frontier press release, Solar Frontier Sets Thin-Film PV World Record with 20.9% CIS Cell. April 2, 2014, http://www.solar-frontier.com/eng/news/2014/C031367.html (accessed May 2014).
(26) Ishizuka, S.; Yamada, A.; Fons, P. J.; Shibata, H.; Niki, S. Impact of a Binary Ga_2Se_3 Precursor on Ternary $CuGaSe_2$ Thin-Film and Solar Cell Device Properties. *Appl. Phys. Lett.* **2013**, *103*, 143903-1−5. Ishizuka, S.; Yamada, A.; Fons, P. J.; Shibata, H.; Niki, S. Erratum. *Appl. Phys. Lett.* **2013**, *103*, 269903.
(27) Ishizuka, S.; Yamada, A.; Fons, P. J.; Shibata, H.; Niki, S. Structural Tuning of Wide-Gap Chalcopyrite $CuGaSe_2$ Thin Films and Highly Efficient Solar Cells: Differences from Narrow-Gap Cu(In,Ga)Se_2. *Prog. Photovoltaics* **2014**, *22*, 821−829.
(28) Wu, X.; Keane, J. C.; Dhere, R. G.; DeHart, C.; Albin, D. S.; Duda, A.; Gessert, T. A.; Asher, S.; Levi, D. H.; Sheldon, P. 16.5%-Efficient CdS/CdTe Polycrystalline Thin-Film Solar Cell. *Proc. of the 17th European Photovoltaic Solar Energy Conference*, Munich, Germany, 2001; pp 995−1000.
(29) Kranz, L.; Gretener, C.; Perrenoud, J.; Schmitt, R.; Pianezzi, F.; Mattina, F.; La Blösch, P.; Cheah, E.; Chirilá, A.; Fella, C. M.; Hagendorfer, H.; Jäger, T.; Nishiwaki, S.; Uhl, A. R.; Buecheler, S.; Tiwari, A. N. Doping of Polycrystalline CdTe for High-Efficiency Solar Cells on Flexible Metal Foil. *Nat. Commun.* **2013**, *4*, 2306.
(30) Wang, W.; Winkler, M. T.; Gunawan, O.; Gokmen, T.; Todorov, T. K.; Zhu, Y.; Mitzi, D. B. Device Characteristics of CZTSSe Thin-Film Solar Cells with 12.6% Efficiency. *Adv. Energy Mater.*, DOI: 10.1002/aenm.2013014.
(31) Kaufmann, C. A.; Caballero, R.; Eicke, A.; Rissom, T.; Eisenbarth, T.; Unold, T.; Schorr, S.; Stephan, C.; Klenk, R.; Schock, H.-W. Aspects for the Optimization of CIGSe Growth at Low Temperatures for Application in Thin Film Solar Cells on Polyimide Foil. *Conference Record of the 34th IEEE Photovoltaic Specialists Conference*, Philadelphia, PA, 2009; pp 670−675.
(32) Caballero, R.; Nichterwitz, M.; Steigert, A.; Eicke, A.; Lauermann, I.; Schock, H.-W.; Kaufmann, C. A. Impact of Na on $MoSe_2$ Formation at the CIGSe/Mo Interface in Thin-Film Solar Cells on Polyimide Foil at Low Process Temperatures. *Acta Mater.* **2014**, *63*, 54−62.
(33) Gabor, A. M.; Tuttle, J. R.; Bode, M. H.; Franz, A.; Tennant, A. L.; Contreras, M. A.; Noufi, R.; Jensen, D. G.; Hermann, A. M. Band-Gap Engineering in Cu(In,Ga)Se_2 Thin Films Grown from $(In,Ga)_2Se_3$ Precursors. *Sol. Energy Mater. Sol. Cells* **1996**, *41*−*42*, 247−260.
(34) Ishizuka, S.; Yamada, A.; Fons, P. J.; Kamikawa-Shimizu, Y.; Komaki, H.; Shibata, H.; Niki, S. Buried *p-n* Junction Formation in $CuGaSe_2$ Thin-Film Solar Cells. *Appl. Phys. Lett.* **2014**, *104*, 031606-1−4.
(35) Wei, S.-H.; Zhang, S. B.; Zunger, A. Effects of Na on the Electrical and Structural Properties of $CuInSe_2$. *J. Appl. Phys.* **1999**, *85*, 7214−7218.
(36) Mönig, H.; Lockhorn, D.; Aghdassi, N.; Timmer, A.; Kaufmann, C. A.; Caballero, R.; Zacharias, H.; Fuchs, H. Heat Induced Passivation of $CuInSe_2$ Surfaces: A Strategy to Optimize the Efficiency of Chalcopyrite Thin Film Solar Cells? *Adv. Mater. Interfaces*, DOI: 10.1002/admi.201300040.
(37) Hanada, T.; Yamana, A.; Nakamura, Y.; Nittono, O.; Wada, T. Crystal Structure of $CuIn_3Se_5$ Semiconductor Studied Using Electron and X-ray Diffractions. *Jpn. J. Appl. Phys.* **1997**, *36*, L1494−L1497.
(38) Yamazoe, S.; Kou, H.; Wada, T. A Structural Study of Cu-In-Se Compounds by X-Ray Absorption Fine Structure. *J. Mater. Res.* **2011**, *26*, 1504−1516.
(39) Negami, T.; Kohara, N.; Nishitani, M.; Wada, T.; Hirao, T. Preparation and Characterization of $Cu(In_{1-x}Ga_x)_3Se_5$ Thin Films. *Appl. Phys. Lett.* **1995**, *67*, 825−827.